Mitigation of wind-induced vibrations of bridge hangers using tuned mass dampers with eddy current damping

Huawei Niu[*1], Zhengqing Chen[1a], Xugang Hua[1b] and Wei Zhang[2c]

[1]*Key Laboratory for Wind and Bridge Engineering of Hunan Province, College of Civil Engineering, Hunan University, Changsha 410082,, Hunan, China*
[2]*Department of Civil and Environmental Engineering, University of Connecticut, Storrs, CT 06269, USA*

Abstract. To mitigate vibrations, tuned mass dampers (TMD) are widely used for long span bridges or high-rise buildings. Due to some durability concerns, such as fluid degradation, oil leakage, etc., the alternative solutions, such as the non-contacted eddy current damping (ECD), are proposed for mechanical devices in small scales. In the present study, a new eddy current damping TMD (ECD-TMD) is proposed and developed for large scale civil infrastructure applications. Starting from parametric study on finite element analysis of the ECD-TMD, the new design is enhanced via using the permanent magnets to eliminate the power need and a combination of a copper plate and a steel plate to improve the energy dissipation efficiency. Additional special design includes installation of two permanent magnets at the same side above the copper plate to easily adjust the gap as well as the damping. In a case study, the proposed ECD-TMD is demonstrated in the application of a steel arch bridge to mitigate the wind-induced vibrations of the flexible hangers. After a brief introduction of the configuration and the installation process for the damper, the mitigation effects are measured for the ambient vibration and forced vibration scenarios. The results show that the damping ratios increase to 3% for the weak axis after the installation of the ECD-TMDs and the maximum vibration amplitudes can be reduced by 60%.

Keywords: eddy current damping tuned mass damper (ECD-TMD); arch bridges; hanger; tuned mass damper; wind-induced vibration; vibration control

1. Introduction

Large vibrations of slender steel hangers have been one of the major concerns for the design of long-span arch bridges or suspension bridges, which could be critical for the bridge safety, serviceability, and durability. Many large amplitude vibrations of hangers were reported since 1980s (Ulstrup 1980). In the 1990's, most of the H section hangers of the Jiujiang Yangtze River Bridge, China were found vibrating with large amplitudes at a low wind speed of 8 m/s (Gu *et al.* 1994). More recently in 2006, large torsional wind-induced vibrations of H-shaped steel hangers of Dongping Bridge, China, were observed. More than 20 hangers vibrated violently for over 20 hours leading to severe cracks on the flanges near the hanger-girder connections for all the 13 longest hangers (Chen *et al.* 2010, 2012). Many mitigation plans were proposed, such as using perforations on the web or the flange (Ma *et al.* 2005), wind-resistant cables (Chen *et al.* 2012), tuned mass dampers (Gu *et al.* 1994, Li *et al.* 2012) etc. However, these mitigation measures generated new problems. For example, perforations on the web or the flange may increase the galloping critical velocity, and no obvious effects were found for flutter instability and vortex shedding excitation. Connecting the hangers using wind-resistant cables is effective to increase the critical velocity of hangers. However, the adverse effects on bridge aesthetics limited its wider applications.

In addition to these vibration control measures, the turned mass dampers (TMDs) (Tamura 2008, Fujino 2002, Spencer and Nagarajaiah 2003, Lin *et al.* 2010, Pourzeynali and Esteki 2009, Zhu *et al.* 2016), as one type of passive mitigation method, have been widely used for many civil infrastructures, as well, especially for long span bridges to suppress the wind-induced vibrations (Koshimura *et al.* 1994, Fujino and Yoshida 2002, Larsen *et al.* 1995, Chen and Kareem 2003, Chang *et al.* 2003). A typical TMD include a lumped mass, a spring element, and damping elements to dissipate the vibration energy (Soong *et al.* 1997). Traditionally, the damping in a TMD is provided by the viscous dampers, oil tanks or frictions. However, some researchers found the fluid dampers were susceptible to fluid degradation and sealing over time (Wang *et al.* 2012; Sodano and Bae 2004, Amjadian and Agrawal 2017). For example, the San Francisco–Oakland Bay Bridge and the Vincent Thomas Bridge were found with the leakage problems for their dampers during their inspections (Konstantinidis *et al.* 2011). Meanwhile, with a large start-up force caused by friction inside the fluid or friction

∗Corresponding author, Associate Professor
 E-mail: niuhw@hnu.edu.cn
[a] Professor
 E-mail: cexghua@hnu.edu.cn
[b] Professor
 E-mail: cexghua@hnu.edu.cn
[c] Assistant Professor
 E-mail: zqchen@hnu.edu.cn

dampers, many TMDs does not work for small amplitudes of vibrations of the building, such as the TMD in the Taibei 101 Tower. Nevertheless, the temperature-sensitive damping properties of fluids increased the uncertainty of the damping effects for different seasons, which endanger the control performance of the TMD (Weber and Feltrin 2010).

In parallel, eddy current tuned mass damper system have been developed and used in many fields other than large scale civil engineering projects, such as the magnetic braking system and in the vibration control devices for the rotating machinery (Sodano and Bae 2004, Anantha Krishna and Sathish Kumar 2018), and wind tunnel testing, such as in the BLWT Laboratory at University of Western Ontario, Canada and Hunan University, China. In an ECD system, the circulating eddy currents are generated in a conductor when there is a relative motion between the conductor and magnetic field. A resistive force will cause energy dissipation due to the electrical resistance. The resistive force induced by the eddy currents is proportional to the relative velocity. Therefore, the damping system can be described as a form of viscous damping, as well. After development of this damping mechanism, many theoretical simulations and experimental investigations were carried out, which show their excellent control performances of ECD (Sodano *et al.* 2005, 2008). With many followed studies and applications (Wen *et al.* 2016, Lu *et al.* 2018, Amjadian and Agrawal 2018, David Saige *et al.* 2017), the feasibility of the non-contact strategy for mitigations of wind-induced vibrations of flexible bridge elements have demonstrated their strong potential especially at a very low wind speed due to the non-frictions of the ECD-TMD. Without liquids and seals, a better durability is expected comparing with the traditional fluid-based TMDs. To apply such ECD-TMD concept from a small and lab scale to a scale for the real long-span bridge, lots of experimental testing and sensitivity analysis were carried out in the present study. Therefore, seeking for a better alternative to the current ECD technique is the motivation of the present study.

The present study focused on the development of an innovative passive TMD with eddy current damping induced by permanent magnets. This paper is organized as the following. After introduction, basic theories for ECD and TMD parameter will be briefly introduced. Secondly, the structure and main elements of the designed ECD-TMD as well as numerical analysis for ECD configuration are presented. After demonstration of the application of the ECD-TMD to suppress the wind-induced vibration of long hangers, and the implementation process of these ECD-TMDs on the site, the control effects of the ECD-TMDs were discussed based on the field experiments.

2. Modelling of ECD-TMD

A hanger with a TMD subjected to harmonic excitation can be described by a two-degree-of-freedom system, as shown in Fig. 1. The dynamic motion equations for this system can be written as (Soong and Dargush 1997)

$$
\begin{bmatrix} m_p & 0 \\ 0 & m_\alpha \end{bmatrix} \begin{bmatrix} \ddot{x}_p(t) \\ \ddot{x}_\alpha(t) \end{bmatrix} + \begin{bmatrix} c_p + c_\alpha & -c_\alpha \\ -c_\alpha & c_\alpha \end{bmatrix} \begin{bmatrix} \dot{x}_p(t) \\ \dot{x}_\alpha(t) \end{bmatrix} +
$$
$$
\begin{bmatrix} k_p + k_\alpha & -k_\alpha \\ -k_\alpha & k_\alpha \end{bmatrix} \begin{bmatrix} x_p(t) \\ x_\alpha(t) \end{bmatrix} = \begin{bmatrix} F_0 \\ 0 \end{bmatrix} \sin(\omega t) \tag{1}
$$

in which $x_p(t), \dot{x}_p(t), \ddot{x}_p(t)$ and $x_\alpha(t), \dot{x}_\alpha(t), \ddot{x}_\alpha(t)$ are the vibration displacement, velocity, acceleration of the hanger and the TMD; m_p, k_p, c_p and $m_\alpha, k_\alpha, c_\alpha$ are the modal mass, stiffness, damping coefficients of the hanger and the TMD respectively; F_0 and ω are the amplitude and circular frequency of the excited force.

For the hanger-TMD system, the dynamic magnification factor (DMF) by displacement R can be determined as

$$
R = \sqrt{\frac{\left(\beta^2 - \alpha^2\right)^2 + (2\xi\beta)^2}{\left[(\beta^2 - \alpha^2)(1 - \alpha^2) - \mu\beta^2\alpha^2\right]^2 + [(2\xi\beta)(1 - \beta^2 - \mu\beta^2)]^2}} \tag{2}
$$

where μ is the mass ratio between the added mass of TMD and the hanger; ξ is the damping ratio, $\xi = c_\alpha / (2m_\alpha\omega_\alpha)$; α is the frequency ratio of the TMD to the hanger; β is the frequency ratio of the excitation force to the natural frequency of the hanger.

Derived from the fixed points of DMF curve, the TMD optimal frequency ratio α_{opt} and the optimal damping ratio ξ_{opt} can begiven as (Warburton 1982, Rana and Soong 1998)

$$
\alpha_{opt} = \frac{1}{1 + \mu} \tag{3}
$$

$$
\xi_{opt} = \sqrt{\frac{3\mu}{8(1 + 3\mu)}} \tag{4}
$$

When the damping is generated by an ECD system, such as shown in Fig. 2, the damping force and the damping coefficients in the velocity direction due to the eddy currents can be obtained (Sodano *et al.* 2006, Wang *et al.* 2012)
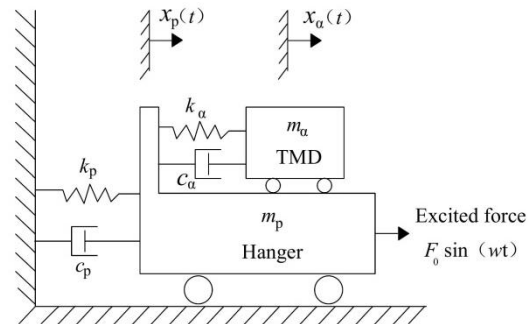

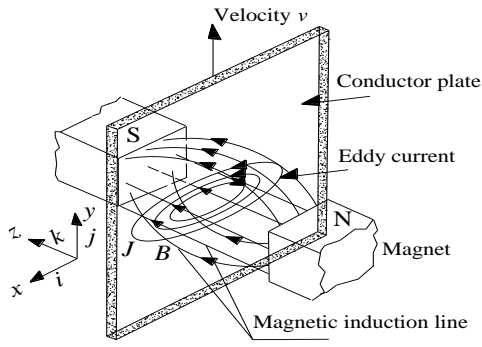Fig. 1 Two degree-of-freedom modelling of the hanger and TMD system

Fig. 2 Schematic of generated eddy current by the conductor plate moving with a magnetic field

$$F_{vy} = -\sigma v_y \int_v (B_X^2 + B_Z^2) dV \qquad (5)$$

$$C_{vy} = -\sigma \int_v (B_X^2 + B_Z^2) dV \qquad (6)$$

where σ is the electrical conductivity of the conductive plate; V is the relative velocity between the permanent magnets and the conductive plate; and B is the magnetic flux density due to the permanent magnets. It can be seen that the induced damping force and damping coefficient are proportional to the relative velocity between the permanent magnets and the conductive plate, and the damping force and damping coefficient in y direction is only dependent on the components of the magnetic flux density in x direction and z direction. Therefore, the permanent magnets should better be magnetized in x direction or z direction to achieve larger damping coefficient with a given size of damping device.

For an ECD-TMD, if the added muss m_α and circular frequency ω_α are obtained previously, the damping ratio of TMD can be determined as

$$\xi_{TMD} = \frac{c_{vy}}{2m_\alpha \omega_\alpha} \qquad (7)$$

3. Design of the ECD-TMD

The proposed eddy current damping TMD (ECD-TMD) consists of an outer frame, a cantilever beam, two lumped mass blocks and an ECD system, as shown in Fig. 3. Here, the plates to fix the nylon columns in the real model are omitted in the sketch to show the main parts more clearly. Compared with the aforementioned references, the ECD-TMD has two improvements: (1) a new configuration of ECD system that the magnets are placed in one side of the conductive plates which could easily adjust the damping through changing the gap; (2) a cantilever beam with uniform strength, which improves the anti-fatigue performance of the stiffness element of the TMD.

3.1 Design of ECD system

For an ECD system in the TMD used on a bridge, three key aspects have to be considered to optimize the design: (1) zero power consumption; (2) higher energy dissipation efficiency especially in the low frequency range (the flexible bridge elements usually have a lower frequency and a lower moving speed, while the energy dissipation amount of the ECD system is related to vibration velocity); (3) easy assembling and adjustment especially in the field. Given this, a new configuration with two rectangular permanent magnets was proposed in the ECD system, as illustrated in Fig. 4, in which the permanent magnets rather than electromagnets were used to avoid any power supply, and the two magnets were arranged at the same side above the conductor plate so that the damping can be adjusted conveniently by changing the gap between permanent magnets and conductor plate. During its operations, the two magnets mounted on the turned mass by the fixed plate will move and induce eddy currents in the conductor plate. In the ECD system, a concentrating flux plate was used to improve the efficiency of energy dissipation, which was further investigated by finite element analysis using COMSOL Multiphysics Software.

The positive effects of a concentrating plate were previously studied by Lequesne *et al.* (1997) to solid-rotor eddy-current couplers and brakes, and by Wang *et al.* (2012) to a large-scale TMD, which proved the feasibility using the concentrating flux plate to improve the damping of a damper.
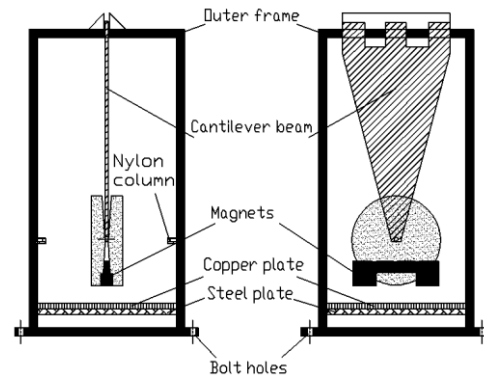

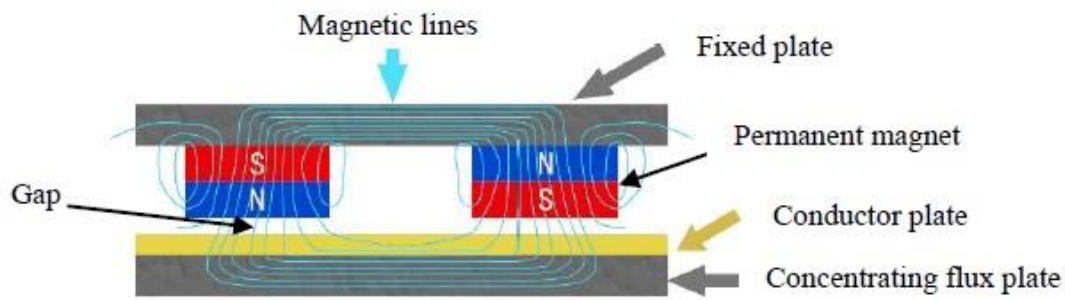Fig. 3 Structure schematic and prototype picture of the ECD-TMD
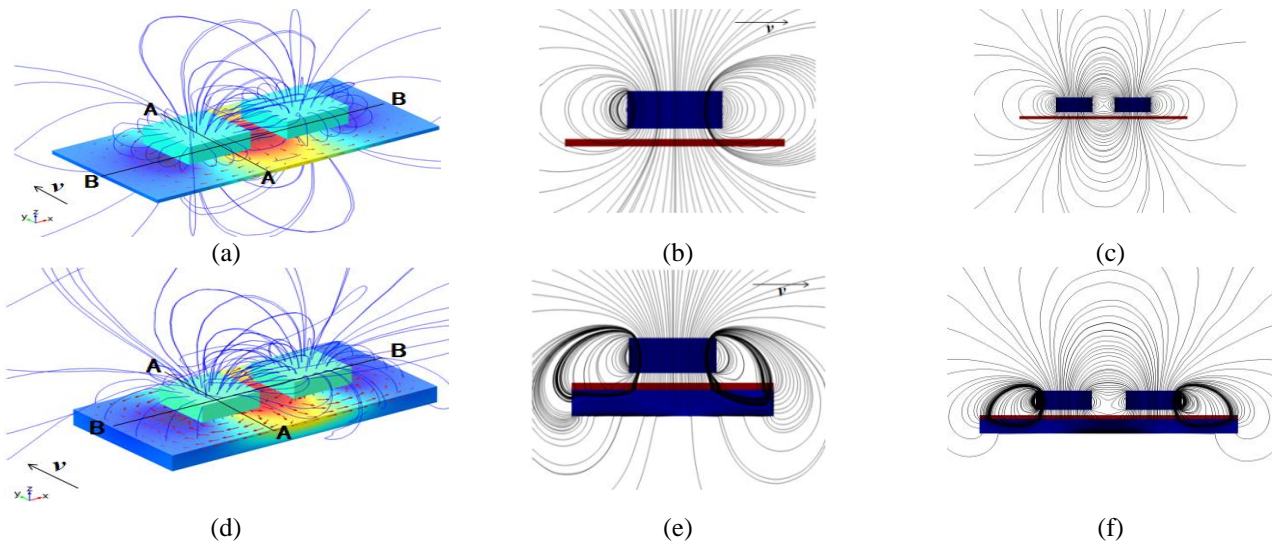
Fig. 4 Sketch of the ECD system in TMD

Fig. 5 Simulated magnetic induction lines with two permanent magnets and copper plate. (a) without steel plate, (b) A-A cross-section, without steel plate, (c) B-B cross-section, without steel plate, (d) with steel plate, (e) A-A cross-section, with steel plate and (f) B-B cross-section, with steel plate

To further investigate the effects, two rectangular permanent magnets and a common steel plate used as concentrating flux plate, as shown in Fig. 4, were simulated by COMSOL software. At first, mesh sizes were optimized by trial and error with different element mesh sizes until the calculated results were in accordance with the theoretical values (Gou *et al*. 2004, Wang *et al*. 2012). The simulated results with and without the steel plate are compared in Fig. 5. The gathering effects produced by the steel plate are shown clearly by the cross-section along two directions A-A and B-B, and shown as closed circles of magnetic induction lines at the sides of the magnets. Based on the configuration with the steel plate, the damping coefficients C_v or damping forces F_v were investigated. In the calculations, the thickness of the steel plate was defined as 5 mm, and the magnetization intensity M of the magnets was assigned as 1×10^6 A/m referring to the real parameter of the used magnets in TMD, as well as a copper plate was used as the conductor plate.

As shown in Fig. 6, an optimal interval can be found between two magnets corresponding to the maximum damping coefficient C_v. The damping coefficient decreases

with the increasing magnetic gap, which implies the damping ratio of the ECD-TMD can be easily adjusted by varying this gap. In addition, C_v increases first and then decreases with the added thickness of conductor plate, which suggests the necessity of the optimization for the plate thickness. The linear relationship is found for the damping force and relative speed in most conditions. However, the nonlinear relationship becomes dominant with the increases of thicknesses or relative speeds. The calculated results serve as the design guidance of the ECD system for TMDs described hereinafter.

Referring to the previously calculated results, the ECD system was designed to include two permanent magnets, one copper plate, and one steel plate. The sketch of the ECD system is shown in Fig. 4. The thicknesses of the copper plate and steel plate are both 5 mm. To easily adjust the damping ratio of TMD, the copper plate is attached on the upper surface of the steel plate. Therefore, the gap between the magnets and the copper plate can be changed from 0 to 15 mm. The two magnets were embedded at the bottom of the lumped mass blocks and the interval between them is 25 mm.
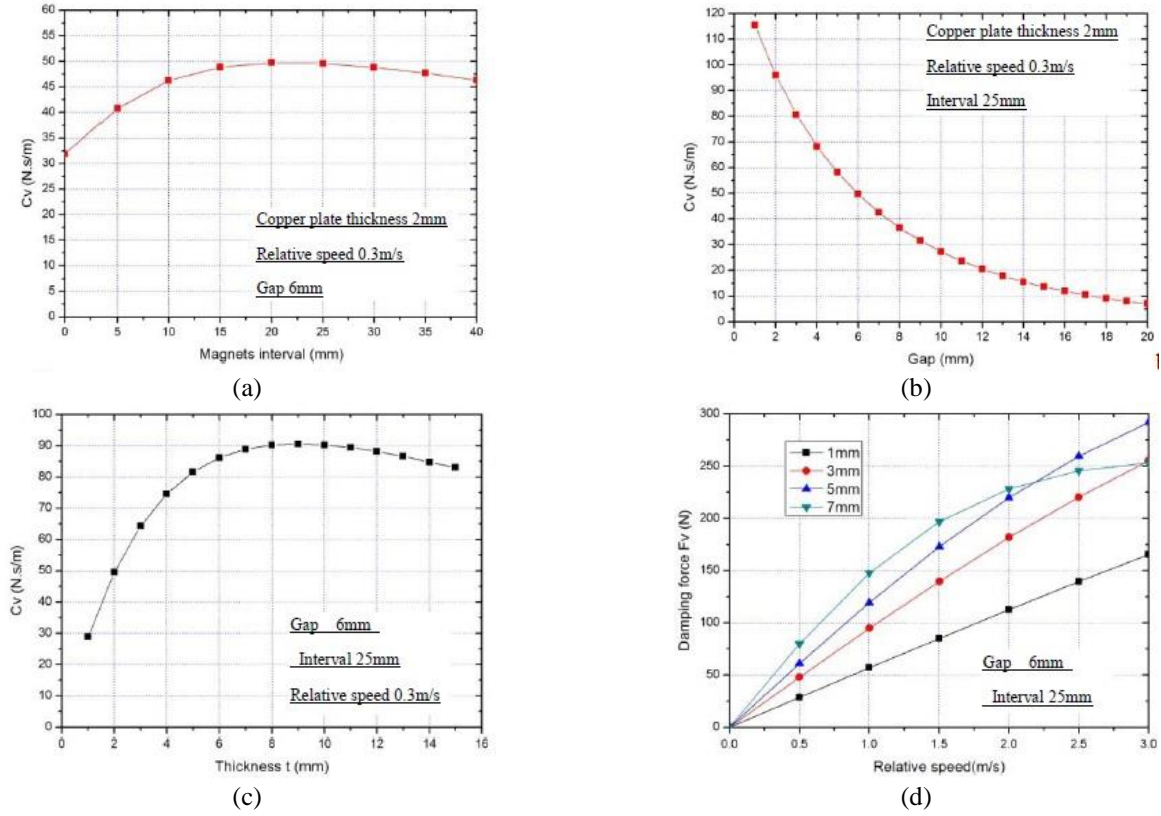
Fig. 6 Calculated eddy current damping coefficients or damping forces with different parameters. (a) interval between two magnets, (b) gaps between magnets and copper plate, (c) copper plate thickness and (d) relative speeds and copper plate thicknesses

3.2 Design of stiffness element

To improve fatigue performances, the cantilever beam with uniform strength is adopted as stiffness components, which is effective to avoid the root damage due to stress fatigue. According to the theory of the uniform strength beam, the width $b(x)$ of the cantilever beam with a rectangular section can be given by

$$b(x) = 6k_\alpha \delta_{\max} x / \sigma_{\max} h^2 \qquad (8)$$

where k_α is the effective stiffness of the beam, $k_\alpha = m_\alpha \omega_\alpha^2$; $\sigma_{\max}$ is the allowable stress corresponding to the steel fatigue; x is the distance from the designed point to the tip of the cantilever beam; $\delta_{\max}$ is allowable maximum displacement of the lumped mass blocks; m_α are the moving masses including the cantilever beam and the lumped mass blocks with two magnets; ω_α are the circular frequency of the TMD; h is the thickness of the steel plate used for the cantilever beam. The preliminary parameters of the cantilever beam can be calculated, and the final parameters were evaluated and optimized based on the FEA results. In addition, in order to prevent the overload conditions that may cause fatigue issues, two nylon short columns are mounted on the outer frame to limit the maximum displacement of the cantilever beam.

As illustrated in Fig. 3, the cantilever beam was riveted at the top of the outer frame of which the foot would be anchored on the central diaphragm plate of hangers. To meet the requirement of adjusting the frequency deviation derived from the difference between the FEM analysis and the field test, the top end of the cantilever beam is reserved as 100 mm long which can be used to adjust the TMD frequency according to the tested frequency of a hanger.

3.3 Design of the tuned mass

As illustrated in Fig. 3, the lumped mass blocks were fixed at the tip of the cantilever beam so that it enables the frequency of the TMD to be tuned easily. To ease frequency adjustments, additional reserved space is reserved for a steel plate to adjust the total lumped mass at the two sides of the mass blocks.

Due to the strength and space limitation of the hangers, the total weight is strictly limited under 50 kg for an easy move by one or two workers, considering future maintenance and repair. According to the pre-defined mass ratio μ, the required TMD masses may still surpass this limitation. In this circumstance, the required concentrated masses can be divided into two or more ECD-TMDs in the real application.

Fig. 7 General view of the Rongjiang Steel Arch Bridge

Table 1 Basic parameters of all types of the hanger

Hanger Parameter/No.	G13A13	G14A14	G15A15	G16A16	G17A17	G18A18	G19A19	G20A20
Length (m)	10.313	19.250	26.813	33.000	37.813	41.250	43.313	44.000
λ_{across}	12	23	32	39	45	49	51	52
λ_{along}	16	29	41	50	57	63	66	67
Total mass (kg)	1773.5	3535	4191.2	5320.5	6072.9	6634.3	6963.3	7066.3

4. Case study

4.1 Description of the Rongjiang Steel Arch Bridge

Rongjiang Steel Arch Bridge is across the Rongjiang River, located in Shantou, China, as shown in Fig. 7. The bridge's total length is 660 m consisting of two main spans of 220 m and two side spans of 110 m. A steel truss girder was used, which comprises of two main trusses with an interval and height of both being 15 m. The rise-to-span ratio of the two arches is 1/5. The arch follows a second-degree parabola line. The heights of two arch tops over the upper chord of truss girder are 44 m. To keep the smooth running of the high-speed train, a total of 60 rigid hangers are used for the two arches. These hangers are grouped into eight types by their lengths, as shown in Table 1. All the hangers have the same rectangular cross-sections of 1.082 m (across bridge)×0.824 m (along bridge), and the longest hanger is 44 m with the slenderness ratio across bridge 52 and along bridge 67.

4.2 Wind-resistant stability assessment of the hangers

For the bridge, the vertical steel hangers are the vital structural elements. With a large slenderness ratio and the typical rectangular-shaped cross section, these hangers are prone to wind induced vibrations, especially for the wind-induced vortex shedding and galloping. In addition, the bridge locates in a typhoon prone region and the bridge site is just 30 km away from Shantou Bay. The design wind speed at 10 m height is 39.4 m/s. With an additional elevation difference of 57 m between the arch foot and the design water level, the design wind speed for hangers corresponding to half height of the arches reaches 54.5 m/s. Therefore, it is critical for the wind-resistant stability design of the hangers. At the initial design phase of the bridge, wind tunnel tests were carried out to understand wind structure interactions.

Since cross sections of all hangers are the same, the longest hanger numbered G20A20 was selected for further investigation of wind-induced vibrations due to its slenderness. A rigid 1/5-scale sectional model was designed for the experiment. The cross section is 0.216×0.165 m, and the length of the model is 1.53 m. The experimental wind flow is uniform, and the turbulence intensity is less than 1%. Both the static aerodynamic force coefficients and wind-induced vibration tests were performed in HD-2 Wind Tunnel of Hunan University, China. The tested aerodynamic force coefficients and wind-induced vibrations for the longest hanger are illustrated in Fig.8. Since the hanger is vertical, the yaw angle for the bridge deck turns into the wind attack angle for the hanger. In the wind tunnel tests, the wind attach angles β were measured from 0~90°. Specifically, β=0°is corresponding to across wind direction for the bridge deck, which means that the wind direction is along the strong axis of the hanger. Meanwhile, the β=90°means the wind direction is along the weak axis of the hanger.

Based on the experimental results, the main instability problem for the hangers is related to the coupling vortex-induced vibration and galloping (Niu *et al.* 2015), which needs to be further studied. In the present work, a simple
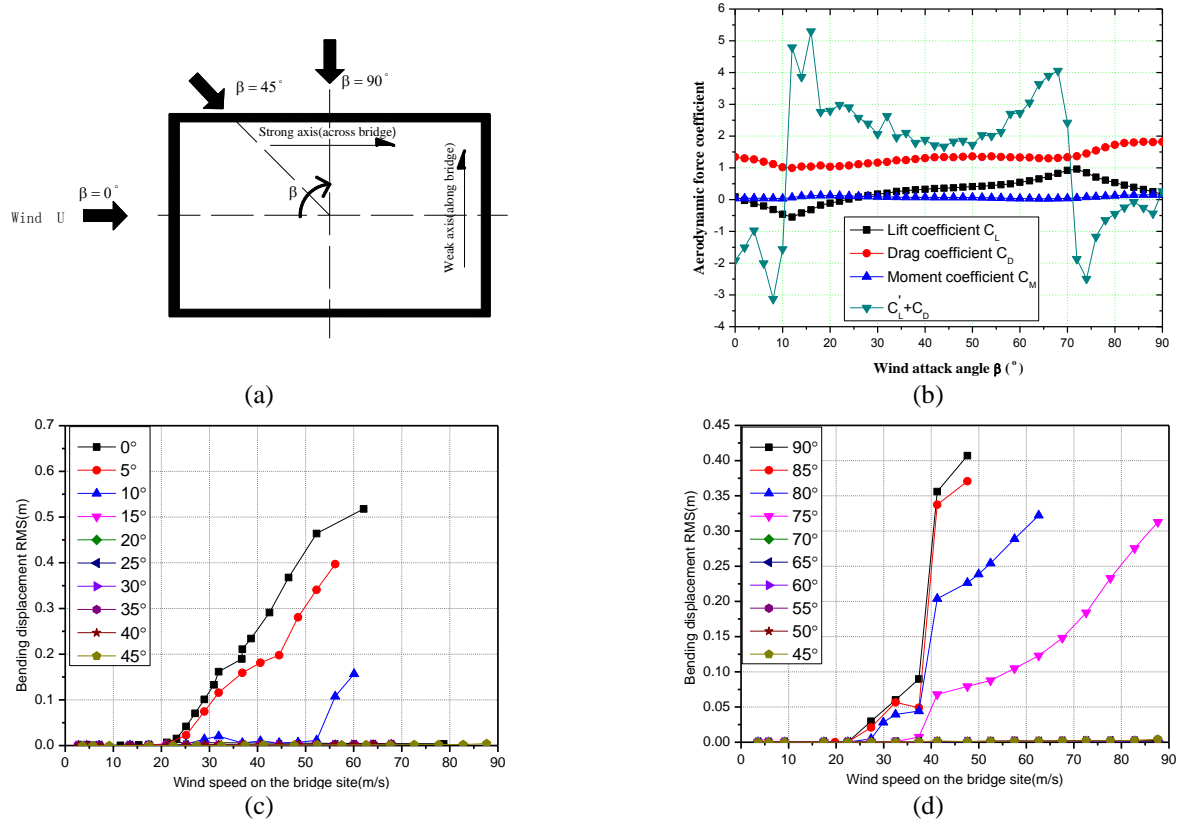
Fig. 8 The wind tunnel test results of aerodynamic force coefficients and wind-induced bending responses (a) definition of the wind attack angle *β*, (b) aerodynamic force coefficients, (c) wind-induced responses along weak axis and (d) wind-induced responses along strong axis

Table 2 Evaluated Critical Wind Speeds of the Hangers Numbered G_iA_i *(i=16~20)*

Hanger Number	Axis	G13A13	G14A14	G15A15	G16A16	G17A17	G18A18	G19A19	G20A20	Checking speed (m/s)
Vortex-induced resonance onset wind speed (m/s)	Strong	352	132	71	**43**	**31**	**25**	**25**	**24**	*54*
	Weak	309	115	56	**37**	**29**	**25**	**23**	**22**	
Galloping wind speed (m/s)	Strong	960	360	194	116	84	69	67	**64**	*65*
	Weak	347	129	68	**42**	**32**	**27**	**25**	**24**	

method is employed to assess the instability of the hangers, which separately evaluates the onset wind speeds of the vortex-induced vibration and the critical wind speeds of the galloping through measured Strouhal number and galloping coefficient. The onset wind speed of vortex-induced vibration U_{cr} and the critical wind speed of galloping V_{cg} can be determined as (Simiu and Scanlan 1996)

$$U_{cr} = \frac{f_v D}{St} \qquad (9)$$

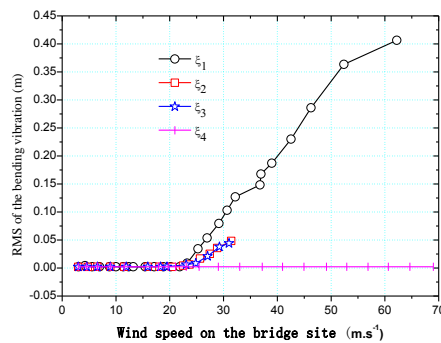$$V_{cg} = -\frac{4m\omega\xi}{\rho D} \cdot \frac{1}{C_L' + C_D} \qquad (10)$$

where D is the length of the side of the rectangular cross-section normal to mean flow velocity; f_v is the vibration frequency of the hanger, which is calculated by finite element method; St is the Strouhal number that is calculated by the measured onset wind velocity through hanger G20A20 model at 0° and 90°, 0.112 and 0.163 respectively; m is mass per unit length of the hanger; ω is the circular frequency of the hanger; ξ is modal damping ratio of the hanger; ρ is air density; $C_L' + C_D$ is Den Hartog coefficient, as illustrated in Fig. 8(b)). Considering the natural wind direction varying with turbulence, the mean values of Den Hartog coefficients of -1.85 and -0.85 at 0°~10°and 72°~90° are used to evaluate the critical wind speed of galloping. The evaluated results of critical wind speeds are listed in

Table 2, which shows the critical wind speeds of the hangers numbered G16A16~G20A20 cannot meet the wind-resistant demands in both direction of strong and weak axis.
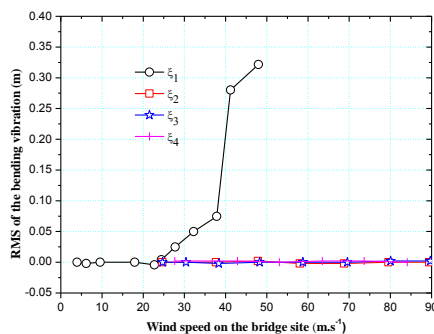
To investigate the effects of damping on the suppression of wind-induced vibrations, the sectional model was further tested by varying damping ratios, and the results were illustrated in Fig. 9. It was found that the necessary damping ratios to control the wind-induced vibration of the long hanger are 0.01 at strong axis and 0.03 at weak axis respectively, which provided the reference data for ECD-TMD design and vibration control performance assessment.

4.3 Design parameters for an ECD-TMD

To get the target mass ratio μ, the complex eigenvalue analysis to the model of coupled hanger-TMD system was carried out. Corresponding to the aforementioned necessary damping ratios of the system, the mass ratio μ of 0.006 and 0.01 was obtained corresponding to the strong axis and weak axis. Then the damping of TMD ξ_{opt} can be calculated by Eq. (4) and will be realized by the previous ECD system. Considering the total weight and easy installation, the lumped mass for each axis of the hangers numbered G16A16~G20A20 was designed to divide into 2 ECD-TMDs. Therefore, a total of 144 ECD-TMDs will be installed in the entire bridge, as shown in Table 3.

Table 3 Concentrated mass parameters and related numbers for the ECD-TMDs

Hangers Type	Quantity	Needed concentrated mass(kg)		Total number of designed TMD	
		Strong axis	Weak axis	Strong axis	Weak axis
G16A16	8	31.92	63.85	16	16
G17A17	8	36.44	60.73	16	16
G18A18	8	39.8	66.34	16	16
G19A19	8	41.78	69.63	16	16
G20A20	4	42.4	70.66	8	8

In addition, the frequency is related to the stiffness element of TMD. Therefore, the control efficiency of the TMD is very sensitive to the frequency ratio between the TMD and the main structure. During the design of the ECD-TMD, the finite element analysis with a full bridge model and multi-segment hangers was carried out to obtain the frequencies of these hangers. Since the real frequencies of hangers are usually different from the calculated ones obtained from finite element analysis (FEA), in-situ measurements were carried out to find the real frequencies before the design. The onsite implementations of TMDs were divided into several steps to keep up with the construction progress of the two arches and hangers. In the designed construction steps, the main truss girder would be joined first, followed by building the two arches with the hangers one by one. Finally the temporary piers were removed and the concrete decks with tracks were paved. Based on the FEA, the construction stage when one arch with hangers had been completed was selected to obtain the frequencies of the hangers on the field. The frequency of each TMD was fine-tuned to the optimal target value. After that, the fine adjusted ECD-TMDs were installed into the hangers one by one. Finally, when the two arches were both closed, the frequencies and damping ratios of hangers were tested on the site to check and evaluate the control performance of the CED-TMD system.

Considering the symmetry of this bridge, the eleven hangers at the upstream side of the arch to Shenzhen, namely Arch1, were measured using accelerometers, as shown in Fig. 10. During the tests, two accelerometers were installed at the midpoint of each hanger for monitoring the ambient vibrations for the strong axis and the weak axis. The recorded typical acceleration signals and their frequency spectrum of the longest hanger G20A20 are illustrated in Fig. 11, and the vibration frequencies can be obtained easily from the frequency spectrum. The measured frequencies were demonstrated in Table 4 with the calculated frequencies by FEA. Here, different from the beam model that a hanger is simulated by a beam of fixed ends, the full bridge model simulates the boundary conditions of the hangers more accurately by taking account of the main girder and the main arches of the bridge. To investigate the change of these frequencies, these hangers were measured again when the Arch2 were completed and the temporary supports were released, as well as the ECD-TMDs had been installed into these hangers, the results were also listed in Table 4.

(a)

(b)

Fig. 9 Tested results of the longest hanger G20A20 with different damping $\xi1=0.002$, $\xi2=0.01$, $\xi3=0.02$, $\xi4=0.03$. (a) weak axis, 0° and (b) strong axis, 90°
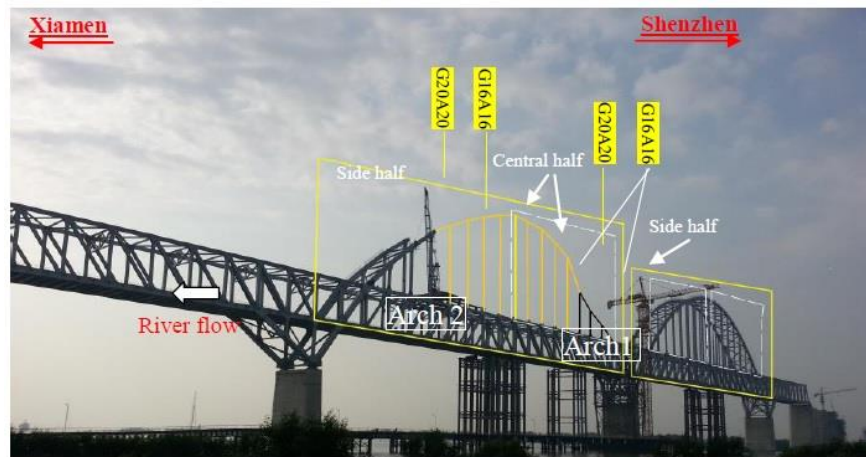
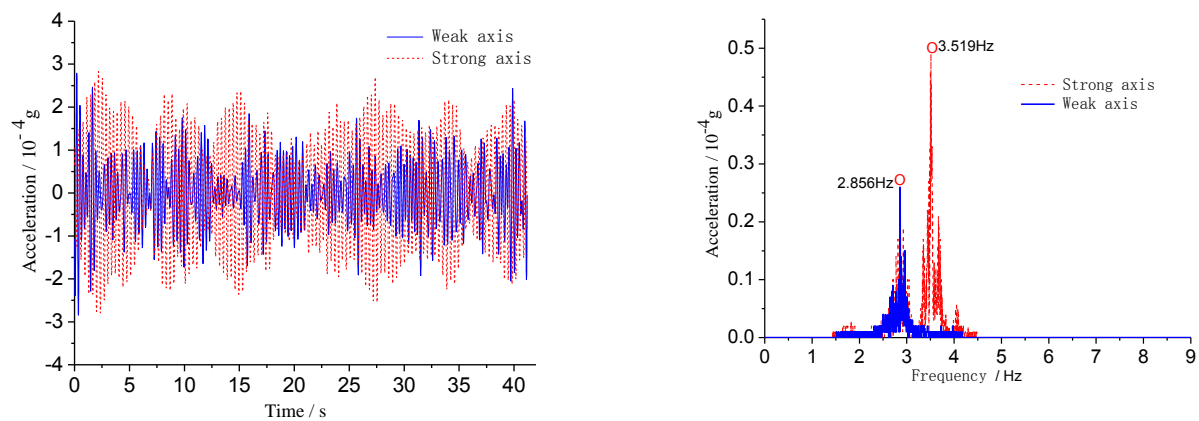Fig. 10 Position diagram for the hangers and the frequency tests

Fig. 11 Acceleration time-history under ambient excitation and the corresponding spectrum of hanger G20A20

Table 4 Frequencies of hangers tested at different positions and situations

Axis	Position & situation description	Hangers No.				
		G16A16	G17A17	G18A18	G19A19	G20A20
Weak axis	Arch1-central half- 1st	5.24	3.78	3.20	2.97	2.86
	Arch1-side half-1st	5.25	3.71	3.18	2.93	2.86
	Arch1-central half-2nd	/	3.89	3.22	2.98	2.90
	Arch2-central half-2nd	5.27	/	3.23	3.17	2.76
	Beam model	5.57	4.29	3.63	3.31	3.21
	Full bridge model	5.05	3.96	3.35	3.07	2.97
Strong axis	Arch1-central half- 1st	5.89	4.30	3.74	3.33	3.52
	Arch1-side half-1st	5.81	4.27	3.72	3.31	3.52
	Arch1-central half-2nd	/	4.54	3.95	3.68	3.47
	Arch2-central half-2nd	5.69	/	3.98	3.71	3.41
	Beam model	7.22	5.55	4.70	4.27	4.15
	Full bridge model	6.45	4.68	3.82	3.75	3.55

*1st test corresponding to the situation only Arch1 was completed, the hanger without TMD; 2nd test corresponding to the situation both Arch1 and Arch2 were completed, the hanger with TMD; "/" refers to no effective data

Table 5 Final Parameters of the ECD-TMDs

	Hanger No.	G16A16	G17A17	G18A18	G19A19	G20A20
Strong axis	Target frequency (Hz)	5.83	4.25	3.70	3.29	3.48
	Tested TMD frequency (Hz)	5.76	4.23	3.69	3.26	3.50
	TMD total weight (kg)	23	30	33	31	33
	Target dampingratio (%)	4.7-6.0	4.7-6.0	4.7-6.0	4.7-6.0	4.7-6.0
	TestedTMD dampingratio (%)	6.05	5.80	5.94	6.25	6.61
Weak axis	Target frequency (Hz)	5.19	3.75	3.16	2.94	2.83
	Tested TMD frequency (Hz)	5.15	3.75	3.16	2.95	2.85
	TMD total weight (kg)	30	38	46	45	46
	Target dampingratio (%)	6-7	6-7	6-7	6-7	6-7
	TestedTMD dampingratio (%)	7.30	6.96	7.01	6.88	7.15

4.4 Installation of ECD-TMDs on the site

To install the ECD-TMDs on these hangers, a diaphragm plate with reserved bolt holes was designed. The plate is welded together with each hanger at the middle point in factory. For the hangers numbered $G_iA_i(i=16\sim20)$, four ECD-TMDs were installed on the diaphragm plates and two ECD-TMDs would vibrate along the strong axis or the weak axis at the diagonal position, as shown in Fig. 12. In fact, two different installation processes were adopted when installing the ECD-TMDs on the hangers in Arch1 and Arch2. For Arch1, the arch with hangers had been completed on the site, therefore, the TMDs had to be lifted by the tower crane and to be dragged into the hanger from the reserved manhole. After that, the TMDs were then mounted on the diaphragm plate; as for Arch2, since the hangers and TMDs were constructed at the same time. The TMDs were pre-mounted on the diaphragm plate and then hoisted together with the hanger to be docked with the arch. Fig. 13 demonstrates the typical situations on the field during the installation process.

4.5 Vibration control performance assessment

Similar to the control performance evaluation method for a cable vibration control system (Chen *et al*. 2004), the modal damping ratios are used to assess the control performance of the supplemental ECD-TMDs. To measure the damping ratio of the hanger with ECD-TMD, two types of experiments were performed on the field, namely, the ambient vibration tests and the forced vibration tests. As aforementioned method to acquire the frequencies of these hangers, the recorded signals of ambient vibrations were also used to identify the needed damping ratio by RDT techniques (Yang 2004, Carlos 2016). Hence the same cases as Table 4 for Arch2 and Arch1 are used to mainly demonstrate the changes of damping ratios with and without ECD-TMDs, as listed in Table 6. For the 1st tests without TMDs in the hangers, the results indicate most of the damping ratios are larger than 0.5%.
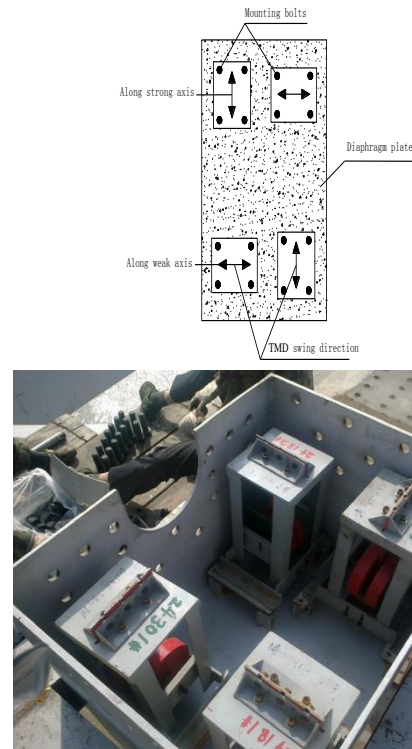

Fig. 12 Installation layout and real picture of four ECD-TMDs on the diaphragm plates

It is worthy to mention that the damping ratios may be related to the influence of the temporary wire rope bracings between two hangers, which are served as a wind-resistance countermeasure during the construction. In addition, the influences derived from the wind-induced aerodynamic damping and the errors of identification method based on ambient excitations are also not neglectable.

To better identify the damping ratios of the hangers, the forced sinusoidal excitations through an eccentric wheel system driven by an electric motor, of which the frequency can be adjusted by a frequency converter, was applied to excite the hanger to vibrate steadily when the excited

frequency was very close to its natural frequency. Due to the limitation of the construction time, only the two longest hangers, numbered G19A19 and G20A20, in Arch2 were tested, as shown in Fig. 14.

In each test, the vibration exciter was first mounted on the surface of the hanger by an electromagnet. Then the frequency converter was adjusted gradually to excite the hanger to a steady vibration. Finally, the exciter was suddenly separated from the hanger by turning off the electricity to the electromagnet. Therefore, the hanger went into a free decay vibration at this time, and the corresponding acceleration time history was recorded to estimate the damping ratio by the logarithmic decrement method. However, due to the interaction of the hanger and the TMD which have two closely-spaced frequencies, the free vibration exhibits beating phenomena. Considering the vibration of the hanger itself was obviously dominant in the signals, the free decay vibration curves were fitted by 1-DOF nonlinear least square method based on the vibration frequency of the hanger. The average value of the damping ratios in the five tests was used as the measured damping ratio for the experimental case. The recorded typical acceleration time histories of the decay vibration are shown in Fig. 15, and the acquired damping ratios are summarised in Table 6.

Fig. 14 Vibration exciter for forced vibration tests of the damping ratios of hanger-TMD System

(a)

(b)

Fig. 13 Typical situations for the TMD installation on the field: (a) installation through the manhole, for Arch1 and (b) pre-installation of ECD-TMDs, for Arch2

Compared to the results from ambient vibration tests, the damping ratios acquired by forced vibration tests have about 10% differences. The differences between the identified damping values can mostly be attributed to three aspects: 1) different approaches, ambient vibration and free decay vibration; 2) different aerodynamic damping due to different wind speed when the tests were performed; 3) different amplitudes, which induced the different signal-to-noise ratio and the damping deviation corresponding to the nonlinear damping-amplitude relationship. However, as shown in the table, the identified damping ratios without ECD-TMDs by the ambient vibration tests are less than the same hanger with ECD-TMDs, and most of the damping ratios with ECD-TMDs are improved more than 1% and 2.5% corresponding to the strong axis and weak axis respectively. Furthermore, the damping ratios acquired by forced vibration tests affirm the beneficial effects of ECD-TMDs, and the results assure the damping ratios of longer hangers being beyond the desired values verified by wind tunnel tests, especially for the weak axis over 3%. Meanwhile, oscillation of the lumped mass blocks of the ECD-TMDs was observed with 3~6 mm amplitude during the forced excitation on the hanger, which proved the ECD-TMDs work in good conditions. To further assess the control effects of the devices, two acceleration sensors along the strong and weak axis were fixed in one of the longest hangers of Arch-1 during the construction stage, and mounted on the diaphragm plates where the ECD-TMDs were mounted. Meanwhile, a propeller anemometer was fixed on the top of the truss girder, where the height above the water level is about 55 m. The recorded typical signals without and with the ECD-TMDs are presented in Fig. 16, in which two wind speed cases are compared.
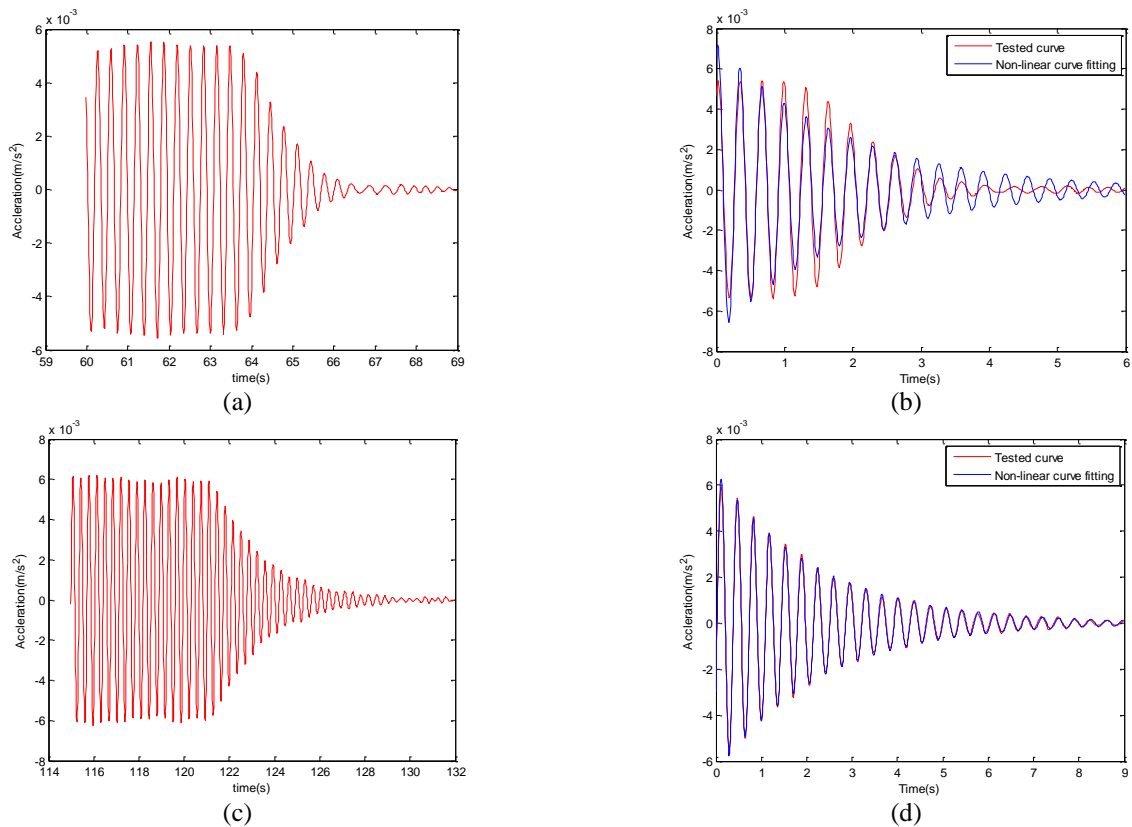
Fig. 15 Typical acceleration time history of the hangers during forced vibration tests, weak axis (a) G19A19, recorded curve, (b) G19A19, fitting curve of the decaying free motion, (c) G20A20, recorded curve and (d) G20A20, fitting curve of the decaying free motion

Table 6 Identified Equivalent Modal Damping Ratios of the Hangers through Field Tests

Axis		Position & situation	G16A16	G17A17	G18A18	G19A19	G20A20
Weak axis	Ambient vibration test	Arch1-central half- 1st	0.0075	0.0065	0.0067	0.0071	0.007
		Arch1-side half-1st	0.0062	0.0084	0.0049	0.0058	
		Arch1-central half-2nd	/	0.0321	0.0308	0.0342	0.0282
		Arch2-central half-2nd	0.0277	/	0.0316	0.0354	0.027
	Forced vibration test	*Arch2-central half-2nd*	/	/	/	*0.0324*	*0.0297*
Strong axis	Ambient vibration test	Arch1-central half- 1st	0.0083	0.0088	0.0074	0.0072	0.0077
		Arch1-side half-1st	0.0092	0.0094	0.0058	0.005	
		Arch1-central half-2nd	/	0.0309	0.0249	0.0228	0.0252
		Arch2-central half-2nd	0.0195	/	0.0275	0.0271	0.0286
	Forced vibration test	*Arch2-central half-2nd*	/	/	/	*0.0206*	*0.0304*

*1st test corresponding to the hanger without TMD; 2nd test corresponding to the hanger with TMD; "/" refers to no effective data

As shown in the figure, the wind induced responses reduced more than 60% after the ECD-TMDs were installed in the long hanger. Moreover, when the Monster Super Typhoon USAGI, reported maximum speed 52 m/s, landed 40km away from the bridge in September 2013, no visible vibrations of these hangers were observed by telescope on the bank. Following that, the bridge also underwent the tropical storm Hagibis in 2014 as well as the severe tropical storm Linfa in 2015, and no special vibrations were reported by the owners. These experiences also proved the feasibility of the ECD-TMDs to suppress the wind-induced vibrations of the slender hangers.
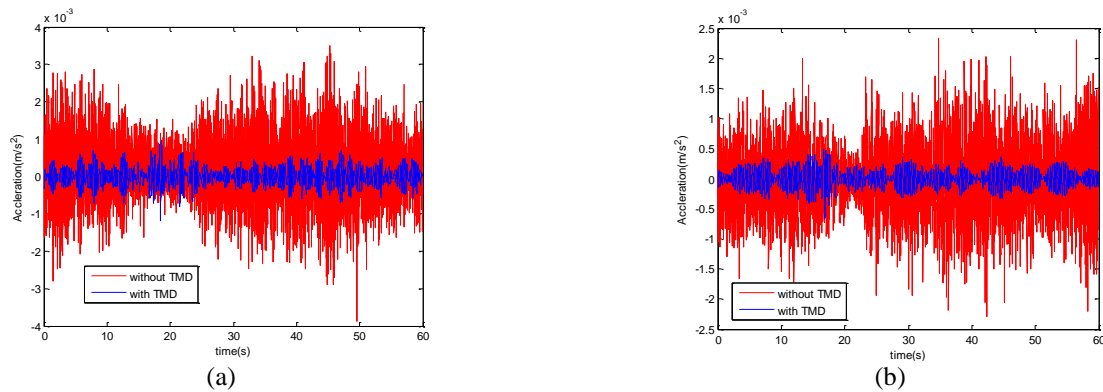
Fig. 16 Recorded typical acceleration time history of the hangers without ECD-TMDs (wind speed, 11.7m/s) and with ECD-TMD (wind speed, 10.6m/s), G20A20: (a) weak axis and (b) strong axis

5. Conclusions

In the present study, a new TMD is proposed that uses the non-contact ECD system to generate damping and dissipate energy for large scale civil infrastructures. A uniform strength cantilever beam is used to mitigate the potential fatigue issues of the beam. Without any viscous damper, oil tank or friction element, the new ECD-TMD is expecting a better durability. Due to its none-friction feature, the new ECD-TMD could also begin to work even at a very low wind speed compared with typical TMDs. With the application of the permanent magnets rather than electromagnets, power supply is not necessary. In addition, the new design of the copper plate with a steel plate has been implemented to improve the energy dissipation efficiency. Nevertheless, the two permanent magnets were arranged at the same side above the copper plate to adjust the damping more conveniently by changing the gap between the magnets and the copper plate. After careful introduction of the ECD-TMD device including the design of the uniform strength cantilever beam, a case study is presented when the ECD-TMD was used to suppress the wind-induced vibrations of the flexible hangers of a steel arch bridge. The TMD parameters, especially the frequencies of ECD-TMDs on the field, were discussed, and the installation process of these ECD-TMDs was introduced, as well. Based on the data from onsite measurements using the ambient vibration and forced vibration method, the wind vibration mitigation were evaluated. The results show that the damping ratios increased more than 1% and 2.5% in the strong axis and weak axis, which is beyond the desired damping ratios, especially for the weak axis over 3%. The ECD-TMDs are also proven to be effective to mitigate the vibrations in the recent several super typhoons. In addition, the proposed ECD-TMD in the bridge not only has a smaller size compared with a conventional oil tank but also has 15% lower cost compared with a conventional oil tank. Meanwhile, the life cycle costs are obviously lower than the conventional oil damper TMD due to the absence of the liquid and the seals. The chances of possible friction issues or fatigue issues are also greatly reduced, which could help improve the durability of these ECD-TMDs.

References

Amjadian, M. and Agrawal, A.K. (2017), "A passive electromagnetic eddy current friction damper (PEMECFD): Theoretical and analytical modelling", *Struct Control Health Monit.*, 2017, e1978, 23 pages, https://doi.org/10.1002/stc.1978.

Amjadian, M. and Agrawal, A.K. (2018), "Modeling, design, and testing of a proof-of-concept prototype damper with friction and eddy current damping effects", *J. Sound Vib.*, **413**, 225-249.

Anantha Krishna, G.L. and Sathish Kumar, K.M. (2018), "Experimental investigation of influence of various parameters on permanent magnet eddy current braking system", Materials Today: Proceedings, 5, 2575-2581.

Bae, J.S., Hwang, J.H., Kwag, D.G., Park, J. and Inman, D.J. (2014), "Vibration suppression of a large beam structure using tuned mass damper and eddy current damping", *Shock Vib.*, Article ID 893914, 10 pages, doi:10.1155/2014/893914.

Bae, J.S., Hwang, J.H., Park, J.S. and Kwag, D.G. (2009), "Modeling and experiments on eddy current damping causedby a permanent magnet in a conductive tube", *J. Mech. Sci. Technol.*, **23**, 3024-3035.

Bae, J.S., Hwang, J.H., Roh, J.H., Kim, J.H., Yi, M.S. and Lim, J.H. (2012), "Vibration suppression of a cantilever beam using magnetically tuned-mass-damper", *J. Sound Vib.*, **331**, 5669-5684.

Carlos, A.P.R., Juan, P.A.S., Hojjat, A., Martin, V.R., David, C.M. and Rene, J.R.T. (2016), "New methodology for modal parameters identification of smart civil structures using ambient vibrations and synchrosqueezed wavelet transform", *Eng. Appl. Artif. Intel.*, **48**, 1-12.

Chang, C.C., Gu, M. and Tang, K.H. (2003), "Tuned mass dampers for dual-Mode buffeting controlof bridges", *J. Bridge Eng.*, **8**(4), 237-240.

Chen, X.Z. and Kareem, A. (2003), "Efficacy of tuned mass dampers for bridge flutter control", *J. Struct. Eng.*, **129**(10), 1291-1300.

Chen, Z.Q., Liu, M.G., Hua, X.G. and Mou, T. M. (2012), "Flutter, galloping, and vortex-Induced vibrations of H-section hangers", *J. Bridge Eng.*, **17**(3), 500-508.

Chen, Z.Q., Liu, M.G., Liu G.D. and Jin, Z.J. (2010), "Wind-induced vibration and wind-resistant design of H-shaped suspenders under large attack angle", *China Civ. Eng. J.*, **43**(2), 1-11 (in Chinese).

Chen, Z.Q., Wang, X.Y., Ko, J.M., *et al.* (2004), "MR damping system for mitigating wind-rain induced vibration on Dongting Lake Cable-Stayed Bridge", *Wind Struct.*, **7**(5), 293-304.

David Saige, W.I., Engelhardt, I.J. and Sebastian Katz, I. (2017), "Application of eddy current damper technology for passive tuned mass damper systems within footbridges", *Procedia Eng.*, **199**, 1804-1809.

Den Hartog, J.P. (1956), Mechanical vibrations, 4th Ed., McGraw-Hill, New York.

Fujino, Y. (2002), "Vibration, control and monitoring of long-spanbridges—recent research, developments andpractice in Japan", *J. Constr. Steel Res.*, **58**, 71-97.

Fujino, Y. and Yoshida, Y. (2002), "Wind-induced vibration and control of Trans-Tokyo BayCrossing Bridge", *J. Struct. Eng.*, **128**(8), 1012-1025.

Gou, X.F., Yang, Y. and Zheng, X.J. (2004), "Analytical expressions of magnetic field distribution of rectangular permanent magnets", *Appl. Math. Mech.*, **25**(3), 297-306.

Gu, J.J., Zhao, Y.C. and Shao, K.H. (1994), "Application of new TMD to suppressing vortex-shedding vibrations of hangers of Jiujiang Bridge over Yangtze river", *China Civ. Eng. J.*, **27**(3), 3-13 (in Chinese).

Keller, P., Higgins, C. and Lovejoy, S. (2014), "Evaluation of torsional vibrations in steel truss bridge members", *J. Bridge Eng.*, 10.1061/(ASCE)BE.1943-5592.0000688, 04014102.

Konstantinidis, D., Kelly, J.M. and Makris, N. (2011), "In-situ monitoring of the force output of fluid dampers, experimental validation, PEER Report 2011/103", Pacific Earthquake Engineering Research Center, University of California, Berkeley.

Koshimura, K., Tatsumi, M. and Hata, K. (1994), "Vibration control of the main towers of the Akashi Kaikyo Bridge", In: Proc. of 1st Int. Conf. on Structural Control, TP3, vol. 2, 98-106.

Larose, G.L., Larsen, A. and Svensson, E. (1995), "Modeling of tuned mass dampers for wind-tunnel tests on a full-bridge aeroelastic model", *J. Wind Eng. Ind. Aerod.*, **54-55**, 427-437.

Larsen, A., Svensson, E. and Andersen, H. (1995), "Design aspects of tuned mass dampersfor the Great Belt East Bridge approach spans", *J. Wind Eng. Ind. Aerod.*, **54-55**, 413-426.

Lequesne, B., Liu, B.Y. and Nehl, T.W. (1997), "Eddy current machines with permanent magnets and solid rotors", *IEEE T. Ind. Appl.*, **33**(5), 1289-1294.

Li, R.Q., Zhu, S.F. and Li, D.C. (2012), "Application of a new type of suspender shock absorber (TLMD) for the nanjing daShengguan yangtze river bridge", *World Bridges*, **40**(6), 68-72 (in Chinese).

Lin, C.C., Lu, L.Y., Lin, G.L. and Yang, T.W. (2010), "Vibration control of seismic structures using semi-active friction multiple tunedmass dampers", *Eng. Struct.*, **32**, 3404-3417.

Lu, Z., Huang, B., Zhang, Q. and Lu, X. (2018), "Experimental and analytical study on vibration control effects of eddy-current tuned mass dampers under seismic excitations", *J. Sound Vib.*, **421**, 153-165.

Ma, C., Liao, H., Zheng, S. and Li, J. (2005), "Wind tunnel experiment on the aerodynamic performances of H-shaped booms", *China Railway Science*, **26**(4), 42-46 (in Chinese).

Niu, H.W., Zhou, S., Chen, Z.Q. and Hua, X.G. (2015), "An empirical model for amplitude prediction on VIV-galloping instability of rectangular cylinders", *Wind Struct.*, **21**(1), 85-103.

Paul, P., Ingale, C. and Bhattacharya, B. (2014), "Design of a vibration isolation systemusing eddy current damper", *J Mech. Eng. Sci.*, **228**(4), 664-675.

Pourzeynali, S. and Esteki, S. (2009), "Optimization of the TMD parameters to suppress the vertical vibrations of suspension bridges subjected to earthquake excitations", *IJE Transactions B: Appl.*, **22**(1), 23-34.

Rana, R. and Soong, T.T. (1998), "Parametric study and simplified design of tuned mass dampers", *Eng. Struct.*, **20**, 193-204.

Ruscheweyh, H. (1996), "Vortex-excited vibrations and galloping of slender elements", *J. Wind Eng. Ind. Aerod.*, **65**(1-3), 347-352.

Shen, W.A., Zhu, S.Y. and Xu, Y.L. (2012), "An experimental study on self-powered vibration control and monitoring systemusing electromagnetic TMD and wireless sensors", *Sensor. Actuat. A*, **180**, 166-176.

Simiu, E. and Scanlan, R.H. (1996), *Wind effects on structures: Fundamentals and applications to design*, 3rd Ed., Wiley, New York.

Sodano, H.A. and Bae, J.S. (2004), "Eddy current damping in structures", *Shock Vib. Dig.*, **36**(6), 469-478.

Sodano, H.A., Bae, J.S., Inman, D.J. and Belvin, W.K. (2005), "Concept and model of eddy current damper for vibration suppression of a beam," *J. Sound Vib.*, **288**(4-5), 1177-1196.

Sodano, H.A., Bae, J.S., Inman, D.J. and Belvin, W.K. (2006), "Improved concept and model of eddy current damper", *J. Vib. Acoust.*, **128**, 294-302.

Sodanoa, H.A. and Inman, D.J. (2007), "Non-contact vibration control system employing an active eddycurrent damper", *J. Sound Vib.*, **305**, 596-613.

Sodano, H.A. and Inman, D.J. (2008), "Modeling of a new active eddy current vibration control system", *J. Dyn. Syst. Meas. Control*, **130**(2), 021009(1-12).

Soong, T.T. and Dargush, G.F. (1997), Passive energy dissipation systems in structural engineering, John Wileys & Sons, New York.

Spencer, B.F. and Nagarajaiah, S. (2003), "State of the art of structural control", *J. Struct. Eng.*, **129**(7), 845-856.

Tamura, Y. (1998). "Application of damping devices to suppress wind-induced responses of buildings", *J. Wind Eng. Ind. Aerod.*, **74-76**, 49-72.

Ulstrup, C.C. (1980), "Aerodynamic lessons learned from individual bridge members". *Ann. N.Y. Acad. Sci.*, **352**(1), 265-281.

Wang, Z.H., Chen, Z.Q. and Wang, J.H. (2012), "Feasibility study of a large-scale tuned mass damper with eddy current damping mechanism", *Earthq. Eng. Eng. Vib.*, **11**(3), 391-401.

Warburton, G.W. (1982), "Optimum absorber parameters for various combinations of response and excitation parameters", *Earthq. Eng. Struct. D.*, **10**, 381-401.

Weber, B. and Feltrin, G. (2010), "Assessment of long-term behavior of tuned mass dampers by system identification", *Eng. Struct.*, **32**, 3670-3682.

Wen, Q., Hua, X.G., Chen, Z.Q., Yang, Y. and Niu, H.W. (2016), "Control of human-induced vibrations of a curved cable-stayed bridge: design, implementation, and field validation", *J. Bridge Eng.*, 10.1061/(ASCE) 1084-0702(2016), **21**(7), 04016028,1-13

Yang, J.N., Lei, Y. and Huang, N. (2004), "Identification of natural frequencies and damping of in situ tall buildings using ambient wind vibration data", *J. Eng. Mech.*, **130**(5), 570-577.

Zhu, J., Zhang, W., Zheng, K.F. and Li, H.G. (2016), "Seismic design of a long span cable-stayed bridge with fluid viscous

dampers", *ASCE Practice Periodical on Structural Design and Construction*, **21**(1):04015006. 10.1061/(ASCE)SC.1943-5576.0000262.

BS